CCFE-PR(15)120

Chu-Chun Fu, M.Yu. Lavrentiev, R. Soulairol, S.L. Dudarev, and
D. Nguyen-Manh

Low- and high-temperature magnetism of Cr and Fe nano-clusters in iron-chromium alloys

Low- and high-temperature magnetism of Cr and Fe nano-clusters in iron-chromium alloys

Chu-Chun Fu,[1] M.Yu. Lavrentiev,[2] R. Soulairol,[1] S.L. Dudarev,[2] and D. Nguyen-Manh[2]

[1]CEA, DEN, Service de Recherches de M´etallurgie Physique, F-91191 Gif-sur-Yvette, France
[2]CCFE, Culham Centre for Fusion Energy, Abingdon, Oxfordshire OX14 3DB, United Kingdom

Low- and high-temperature magnetism of Cr and Fe nano-clusters in iron-chromium alloys

Chu-Chun Fu,[1] M.Yu. Lavrentiev,[2] R. Soulairol,[1] S.L. Dudarev,[2] and D. Nguyen-Manh[2]

[1] *CEA, DEN, Service de Recherches de Métallurgie Physique, F-91191 Gif-sur-Yvette, France*
[2] *CCFE, Culham Centre for Fusion Energy, Abingdon, Oxfordshire OX14 3DB, United Kingdom*

(Dated: September 17, 2014)

Lowest-energy magnetic states and finite temperature properties of Cr nano-clusters in bulk Fe, as well as Fe nano-clusters in bulk Cr, are investigated using density functional theory (DFT) and the Heisenberg-Landau Magnetic Cluster Expansion (MCE) Hamiltonian. We show, by means of non-collinear magnetic DFT calculations, that the magnetic frustration caused by the competing ferro- and antiferro- magnetic interactions either reduces the local magnetic moments or gives rise to non-collinear magnetic structures. Non-collinear magnetic configurations form in the vicinity of very small Fe nano-clusters ($N_{Fe} \leq 5$) if the Fe-Cr anti-ferromagnetic coupling dominates over ferromagnetic Fe-Fe interactions. MCE predictions broadly agree with the DFT data on the low-energy magnetic structures, and extend DFT analysis to larger systems. Non-vanishing cluster magnetization caused by the dominance of Fe-Cr over Cr-Cr anti-ferromagnetic coupling is found in Cr nano-clusters using both DFT and MCE. Temperature dependence of magnetic properties of Cr clusters is strongly influenced by the surrounding iron atoms. A Cr nano-cluster remains magnetic until fairly high temperatures, that is, close to the Curie temperature of pure Fe in the larger cluster size limit. Cr-Cr magnetic moment correlations are retained until high temperatures due to the coupling of interfacial Cr atoms with the Fe environment. Variation of magnetization of Fe-Cr alloys as a function of temperature and Cr clusters' size predicted by MCE is assessed in relation to the available experimental data.

PACS numbers: 75.50.Bb, 75.75.-c, 64.70.kd, 64.75.Op

I. INTRODUCTION

Alloys of magnetic metals with ferromagnetic (FM) and anti-ferromagnetic (AF) ordering tendencies often exhibit complex magnetic properties, bcc Fe-Cr alloys being a representative example of such magnetic materials. Magnetic frustration occurs in regions close to structural defects (surfaces, grain boundaries) and chemical heterogeneities (lattice-precipitate interfaces and small clusters). High-Cr iron alloys are of significant technological interest due to the positive effect of Cr on their corrosion and radiation resistance. Fe-Cr alloys-based ferritic steels have recently attracted attention as candidate structural materials for the next generation fission and future fusion reactors[1–3].

The formation of Cr nano-clusters and precipitates in bcc Fe, and Fe nano-clusters in bcc Cr is a well known phenomenon occurring in Fe-Cr alloys during the so-called $\alpha - \alpha$' phase decomposition. Such decomposition is observed if the chemical content of the alloy is inside the miscibility gap of the binary Fe-Cr phase diagram. Phase decomposition may also be induced or accelerated by irradiation[4]. Magnetic properties of Fe and Cr nano-clusters and precipitates influence the diffusivity of vacancies and solutes[5–8] as well as the Curie temperature of the alloy[9].

Earlier studies explored the effect of magnetic frustration on magnetic ground states of pure or mixed Cr and Mn clusters supported on various metallic substrates (Fe, Cu, Ag) by means of first principles[10–12] and tight binding electronic structure calculations[13,14]. The magnetic structure of clusters was analyzed using both collinear or non-collinear approximations. For instance, using a non-collinear first-principles approach, Bergman *et al.* predicted the occurrence of non-collinear magnetic configurations if antiferromagnetism in a Cr-Mn cluster on the Cu(111) surface was frustrated[10]. Robles *et al.*[13] showed that a tendency to form non-collinear magnetic configurations for Cr clusters supported on bcc Fe is generally weaker than for those supported on fcc Fe substrates. In the former case, magnetic frustration only occasionally gives rise to non-collinear magnetic configurations. Furthermore, by investigating small free-standing Fe-Cr clusters, Longo *et al.*[15] noted a preference for collinear magnetic ordering even in the presence of magnetic frustration. On the other hand, to the best of our knowledge, a detailed investigation of magnetic Cr nano-clusters in bcc bulk Fe at the first-principles level, in particular taking into account both longitudinal and transversal magnetic degrees of freedom, has never been performed. Many *ab initio* studies noted a strong link between magnetism and various thermodynamic, segregation, defect and kinetic properties of Fe-Cr bulk alloys[16–18]. However, magnetic properties of clusters and precipitates were not treated taking into account all the aspects of magnetic complexity, and instead collinear approximation was adopted in Refs.[5,6,19–21].

In a recent paper[22] we investigated interfaces of large precipitates in Fe-Cr alloys and showed that magnetic interactions across a planar Fe/Cr interface can result in the non-collinearity of magnetic moments of Cr atoms with respect to the ferromagnetically ordered moments

of iron atoms, in agreement with experimental neutron diffraction data[23]. Below, using the same simulation methodology, we investigate magnetism of Cr clusters in FM bcc Fe, as well as Fe clusters in AF bcc Cr. Simulations are performed using two complementary techniques, Density functional theory (DFT) and Magnetic Cluster Expansion (MCE). On the one hand, the use of reduced localized basis sets in DFT calculations makes it possible to perform an extensive and systematic *ab initio* study going beyond the collinear approximation. On the other hand, the recently developed MCE model[24,25] has been parameterized and already successfully applied to the study of Fe-Cr alloys, exploring magnetic properties of the alloys in a broad temperature interval[26] as well as the variation of the Curie temperature as a function of chemical composition of the alloys[27]. The broad range of applicability of the MCE model was confirmed by its recent application to fcc Fe-Ni alloys[28]. Magnetic non-collinearity of large Cr clusters found in MCE simulations[29] prompted us to investigate the origin of magnetic order at Fe/Cr interfaces[22]. Good agreement between DFT and MCE results established in that study, now makes it possible to apply the combined DFT and MCE approach to the investigation of non-collinear magnetic properties of Cr and Fe nano-clusters of various shapes and sizes, carried out below.

In what follows we explore how the magnetic structure and energy of Cr(Fe) clusters in bcc Fe(Cr) matrix depend on Fe-Fe, Fe-Cr, and Cr-Cr magnetic interactions. In particular, we investigate if magnetic frustration, resulting from the competing first and second nearest neighbor Fe-Cr anti-ferromagnetic and first nearest neighbor Cr-Cr anti-ferromagnetic interactions, and responsible for the magnetic non-collinearity at planar interfaces[22], also gives rise to non-collinear magnetic configurations of Cr(Fe) clusters.

Extensive DFT calculations of the lowest-energy collinear and non-collinear magnetic structures of small (dimer, trimer etc.) and large nano-clusters, with (100) and/or (110) facets and containing up to 70 solute atoms, were performed to define conditions for the occurrence of non-collinear magnetic configurations. DFT results are also used for validating the MCE model. MCE simulations can describe fairly large clusters, which are beyond the present capacity of DFT calculations. We also study the evolution of magnetic properties as functions of cluster size, starting from very small clusters, where interface effects are important, to fairly large precipitates, where magnetic structure is similar to that of the bulk material. MCE-based Monte Carlo simulations are then used to investigate finite temperature magnetic properties, which are compared with the available experimental information.

The paper is organized as follows. In Section II, we describe the two computational methods used in this study. DFT results are given in Section III and MCE simulations, including the analysis of high temperature properties, are summarized in section IV. Conclusions and summary are given in section V.

II. CALCULATION METHODS

A. First principles approach

First principles calculations were performed using Density Functional Theory (DFT), as implemented in the SIESTA code[30]. In all the calculations alloys are treated as spin-polarized, and the treatment of magnetism goes beyond the collinear approximation. Spin-orbit coupling effects are not taken into account. The validity of non-collinear calculations with SIESTA has already been illustrated earlier[22,31]. The Mulliken population analysis was used to evaluate the atomic magnetic moments. All the results presented in this paper were obtained using the generalized gradient approximation (GGA) exchange-correlation functional in the Perdew-Burke-Ernzerhof (PBE) form[32].

Regarding other DFT approximations, the core electrons are replaced by nonlocal norm-conserving pseudopotentials (NCPP), while the valence ($4s$ and $3d$) electrons are described by linear combinations of numerical pseudo-atomic orbitals. The pseudopotentials and the basis sets for Cr and Fe are the same as in Refs. 7,33,34, where the accuracy of Cr and Fe pseudopotentials and basis sets was tested against the relevant known energy and magnetic properties. They were shown to agree satisfactorily with both the experimental data and accurate DFT values computed using the Projector Augmented Wave (PAW) atomic data[33].

Supercell calculations were performed to model Cr nano-clusters in bcc ferromagnetic (FM) Fe, and Fe nano-clusters in bcc anti-ferromagnetic (AF) Cr. Clusters containing from 2 to 70 atoms were modelled using orthogonal supercells with 128, 250 and 512 atoms.

Calculations were performed assuming constant pressure conditions, i.e. the structures were optimized by relaxing both atomic positions as well as the shape and volume of the supercell. All the residual force and stress components were verified to be less than 0.04 eV/Å and 5 kbar, respectively.

The $k-$point grids used in various supercell calculations were adjusted according to the number of atoms in a cell. The grids were chosen to achieve $k-$space sampling equivalent to a bcc cubic unit cell with a $12 \times 12 \times 12$ shifted $k-$grid. The Methfessel-Paxton broadening scheme with a 0.3 eV width was used. The calculated magnetic structures and cluster formation energies were well converged with respect to the choice of $k-$point grids.

The typical error bar for difference of energies between two magnetic states of a given atomic configuration is estimated to be 0.03 eV.

B. Magnetic cluster expansion

The Magnetic Cluster Expansion (MCE) model was developed in Refs.[24,25] as an extension of conventional Cluster Expansion[35]. Cluster Expansion was successfully used in a study of Fe-Cr alloys[36], where we found that it could only describe chemical order and disorder in the alloy and could not model its magnetic properties. The MCE Heisenberg-Landau type Hamiltonian was then applied[25] to treat both the configurational and magnetic degrees of freedom of the alloy.

The energy of an alloy in MCE depends both on discrete site occupation variables σ_i (for example $\sigma_i = +1$ for Fe, $\sigma_i = -1$ for Cr) and magnetic moments $\mathbf{M}_i$ of the constituent atoms. The magnetic moment vectors have variable direction and magnitude. The MCE Hamiltonian is a sum of conventional Cluster Expansion terms and magnetic terms. The magnetic part of the Hamiltonian has the Heisenberg-Landau form. Magnetic properties of an alloy explicitly depend on its atomic configuration via the site-dependent Landau self-energy terms, which in a self-consistent way determine the magnitudes of atomic magnetic moments, and on the inter-site Heisenberg magnetic interaction parameters. Atomic configurations and magnetic degrees of freedom are not independent, since the magnetic configuration of an alloy depends on its atomic configuration via the dependence of Landau self-energy coefficients A_i, B_i and inter-site Heisenberg exchange interaction parameters J_{ij} on the type of atoms occupying a lattice site, and its nearest neighbor environment. At the same time, the energy of an alloy configuration depends not only on the occupation of lattice sites by atoms of various types but also on the magnitude and orientation of atomic magnetic moments.

In what follows we use an MCE parametrization where only two-atom clusters are retained in the magnetic and non-magnetic parts of the Hamiltonian:

$$\begin{aligned}\mathcal{H}(\{\sigma_i\},\{\mathbf{M}_i\}) &= NI^{(0)} + I^{(1)}\sum_i \sigma_i + \sum_{ij} I^{(2)}_{ij}\sigma_i\sigma_j \\ &+ \sum_i (A^{(0)} + A^{(1)}\sigma_i + \sigma_i \sum_j A^{(2)}_{ij}\sigma_j)\mathbf{M}_i^2 \\ &+ \sum_i (B^{(0)} + B^{(1)}\sigma_i + \sigma_i \sum_j B^{(2)}_{ij}\sigma_j)\mathbf{M}_i^4 \\ &+ \sum_{ij} (J^{(0)}_{ij} + J^{(1)}_{ij}(\sigma_i+\sigma_j) + J^{(2)}_{ij}\sigma_i\sigma_j)\mathbf{M}_i\cdot\mathbf{M}_j. \quad (1)\end{aligned}$$

Here N is the total number of atoms and $I^{(i)}$ are the non-magnetic Cluster Expansion coefficients. Summation over i and j involves atoms occupying nearest neighbor coordination shells. The functional form of equation (1) guarantees that the magnetic self-energy terms, and hence the directions and magnitudes of magnetic moments $\mathbf{M}_i$ predicted by the model, depend on the local environment of each atom. Numerical values of parameters of Hamiltonian (1) for Fe-Cr alloys are given in[25,37]. This Hamiltonian allows fast Monte Carlo simulations over a wide range of atomic and magnetic configurations, concentrations and temperatures.

III. DFT RESULTS AND DISCUSSIONS

A. Cr clusters in FM bcc Fe

We start by investigating Cr nano-clusters in FM bcc Fe. Besides the very small clusters, we consider clusters having the lowest-energy Fe/Cr interfaces, that is, the (100) and the (110) type interfaces found in our previous DFT studies[22]. Four groups of clusters have been examined: (i) small clusters of 2, 3, 4 and 5 Cr atoms, (ii) cubic clusters with (100) facets, containing 9 and 35 Cr atoms, (iii) octahedral clusters with 6, 15, 19 and 24 Cr atoms that present only (110) facets, and (iv) mixed clusters with both (100) and (110) interfaces that contain 13, 14, 16, 18, 22, 41 and 70 Cr atoms. The most relevant configurations of the small clusters are plotted in Fig. 1, and some representative octahedral, cubic and mixed clusters are shown in Fig. 2. A full description of configurations of cubic, octahedral and mixed clusters are given in Table I in terms of the number of Cr atoms in successive atomic planes in a (100) direction.

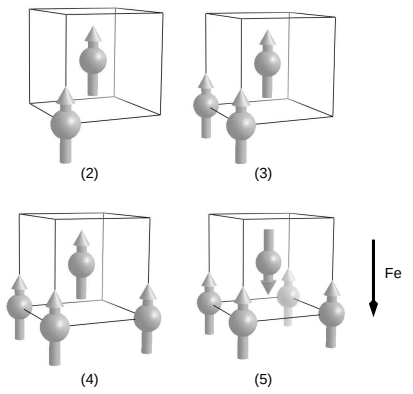

FIG. 1: Schematic representation of atomic positions and atomic magnetic moments (arrows) in small Cr clusters containing between 2 and 5 atoms. Cubic unit cells are drawn with solid lines. The orientation of ferromagnetically ordered collinear Fe lattice magnetic moments is also shown.

To investigate the occurrence and stability of collinear (Col) and non-collinear (NCol) magnetic configurations for a given cluster, we initialized DFT calculations assuming various arrangements of local magnetic moments, in terms of orientations and magnitudes of the moments. As was shown in many previous DFT studies[19,33], an isolated Cr atom in FM-Fe lattice has a large induced magnetic moment, which is anti-parallel to the lattice Fe moments. Such anti-ferromagnetic (AF) coupling tendency between Cr and Fe atoms, particularly between the nearest and next-nearest Fe-Cr neighbours (respec-

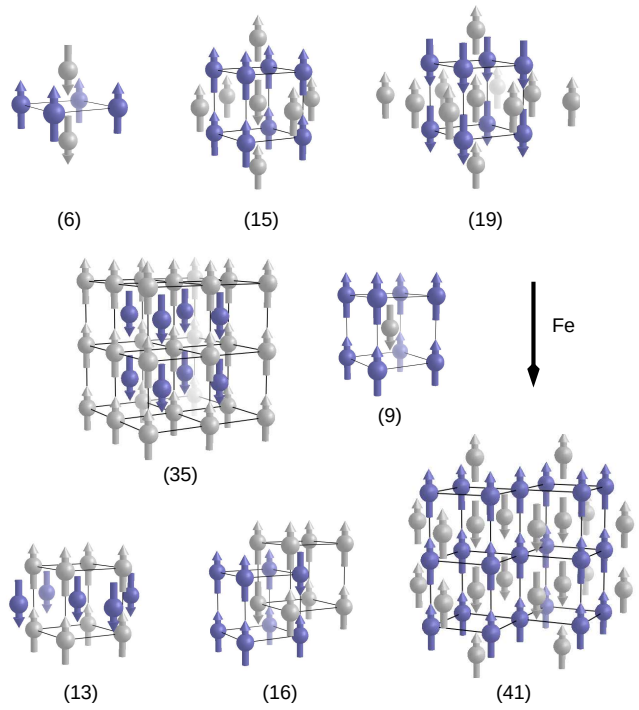

FIG. 2: Schematic representations of atomic positions and atomic magnetic moments (arrows) of some representative Cr clusters in the lowest-energy collinear state. The orientation of Fe magnetic moments is also shown.

Octahedral			
$n = 6$	1-4-1	$n = 19$	1-4-9-4-1
$n = 15$	1-4-5-4-1	$n = 24$	1-4-5-4-5-4-1
Cubic			
$n = 9$	4-1-4	$n = 35$	9-4-9-4-9
Mixed			
$n = 13$	4-5-4	$n = 14$	5-4-5
$n = 16$	4-4-4-4	$n = 18$	4-5-4-5
$n = 22$	4-5-4-5-4	$n = 41$	2-7-8-7-8-7-2
$n = 70$	4-12-13-12-13-12-4		

TABLE I: Structure of octahedral, cubic and mixed Cr n-atom clusters defined by the number of Cr atoms in successive atomic planes in a (100) direction.

tively *nn* and *nnn*), also determines the magnetic configuration of small Cr clusters, where any of the Cr atoms has at most three Cr *nn* (Fig. 1). Because of competition between AF coupling between Fe-Cr and Cr-Cr *nn* pairs in these clusters, the magnitude of moments on Cr atoms decreases with the increasing number of Cr *nn*. This magnitude varies from 2.37 μ_B, 2.05 μ_B, to 0.56 μ_B when the number of Cr *nn* increases from 1 to 3. The particularly small magnitude of the moment on the central atom in a 4-Cr cluster suggests strong magnetic frustration. For the central atom in a 5-Cr cluster with 4 Cr and 4 Fe *nn* (Fig. 1), AF Cr-Cr coupling dominates over Fe-Cr coupling. The local moment on such Cr atom becomes parallel to the Fe moments, and the magnitude of the moment is small (0.95 μ_B). These results are in agreement with previous DFT findings[19] constrained to a collinear approximation. In the present study, we have also verified that there are no other NCol configurations forming as metastable local minima of energy of Cr clusters as functions of orientations of atomic magnetic moments.

For the two cubic clusters with 9 and 35 Cr atoms, all the NCol initial configurations are unstable, and decay to a Col arrangement. This result is consistent with our previous finding that infinite planar Fe/Cr (100) interfaces do not promote magnetic non-collinearity[34]. On the other hand, Cr and Fe local moments tend to be perpendicular to each other across a planar (110) interface, as found in our previous simulations in agreement with experimental data[22,23]. However, for Cr clusters bound by at least one (110) interface, we still find that a Col configuration represents the lowest-energy state for all the cases considered in this study. Moreover, all the NCol initial states decay to the Col ground state for most of the clusters, except for the octahedral clusters with n = 15 and 24, and the mixed clusters with n = 22, 41 and 70, where local minima with NCol arrangements of magnetic moments are found. The energy difference between the Col and NCol states ($E(NColl) - E(Coll)$) of these clusters are all fairly small: 0.09 eV, 0.07 eV, 0.04 eV, 0.17 eV and 0.08 eV respectively. A schematic representation of these NCol structures are shown in Fig. 3.

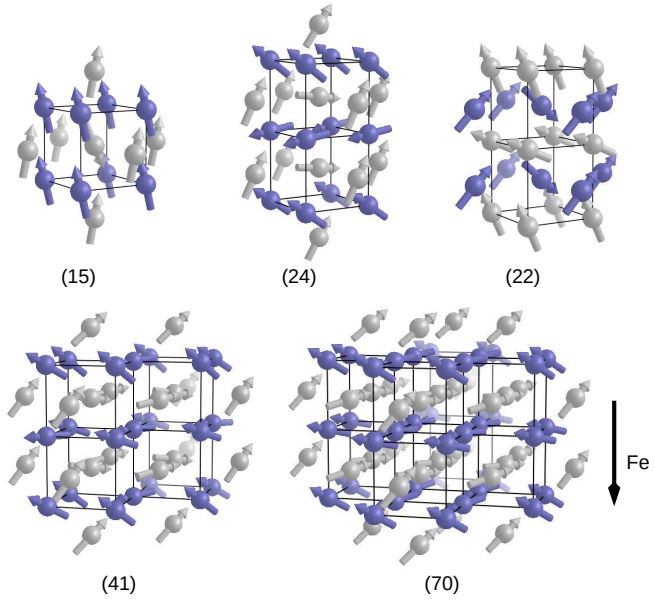

FIG. 3: Schematic representations of atomic positions and local magnetic moments (arrows) of Cr clusters containing 15, 24, 22, 41 and 70 atoms in their metastable NCol configurations. Orientation of the lattice Fe moments is also shown.

It is natural to attempt to rationalize magnetic behaviour of the clusters in terms of magnetic frustration

	6	15	19	24	9	35	13	14	16	18	22	41	70
$<\mu>$ (Col)	1.23	0.51	1.03	0.52	1.97	1.45	0.97	1.62	1.02	0.95	0.62	0.48	0.67
$<\mu>$ (NCol)	-	0.53	-	0.69	-	-	-	-	-	-	0.84	0.85	0.95
M (Col)	0.96	0.46	0.65	0.43	1.61	0.94	0.64	0.98	0.86	0.72	0.52	0.36	0.26
M (NCol)	-	0.47	-	0.44	-	-	-	-	-	-	0.54	0.37	0.29

TABLE II: Average magnitude of magnetic moments of Cr atoms in clusters ($<\mu>=\frac{1}{n}\sum|\mu_i|$), given in μ_B units, and the magnitude (in μ_B) of Cr cluster magnetization ($M=\frac{1}{N_{Cr}}|\sum\mu_i|$), shown as functions of cluster size N_{Cr} for the lowest-energy collinear (Col) and non-collinear (NCol) states. For the Col states, cluster magnetization is anti-parallel to the Fe moments. For the NCol states, the angle between the cluster magnetization and Fe moments varies between 176° and 180°.

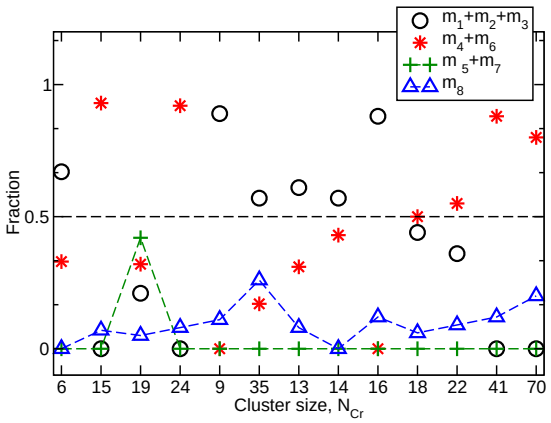

FIG. 4: Fraction of Cr atoms (m_i) with i Cr nearest neighbours (nn) versus the size of Cr cluster (N_{Cr}), for all the octahedral, cubic and mixed clusters studied.

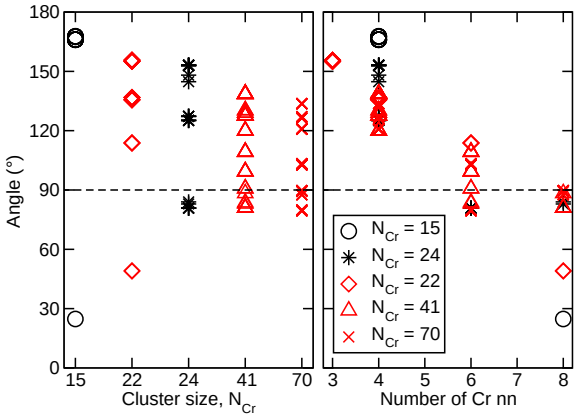

FIG. 5: Absolute value of the angles between local Cr moments and Fe lattice moments in the NCol N_{Cr}-cluster configurations (N_{Cr} = 15, 24, 22, 41 and 70) versus: (left) cluster size, and (right) the number of Cr nn.

and the part played by Cr-Fe interfaces[22]. Coupling between Fe and Cr moments across a planar (110) interface results from competition between two tendencies, leading to magnetic frustration: strong nn and nnn Fe-Cr AF coupling at the interface, and nn Cr-Cr AF coupling in the Cr lattice. For Cr clusters in iron, the situation

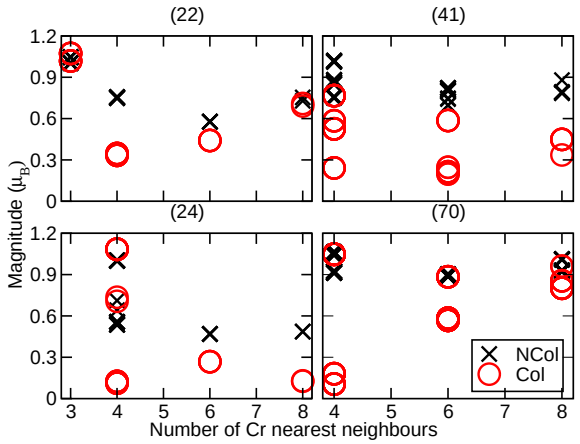

FIG. 6: Magnitudes of local moments on atoms in Col and NCol configurations of n-Cr clusters versus the number of Cr nn.

becomes even more complicated, and size and shape dependent. When a cluster is relatively small and either all or most of the Cr atoms are situated at the interface, the 'interface ordering tendency' of being anti-parallel to the Fe moments clearly dominates over the Cr-Cr AF 'bulk ordering tendency'. This is indeed the case for the smallest N_{Cr} clusters (N_{Cr} = 2 to 6 and n = 14), where none of the Cr atoms has the local bcc-Cr-like environment with all 8 of its nearest neighbours being Cr atoms. The fraction of Cr atoms in each cluster with i Cr nearest neighbours is shown in Fig. 4. For the medium-size clusters, where both interface and bulk tendencies are comparable, the induced magnetic frustration may potentially promote the formation of NCol structures. In practice, there is no simple rule for predicting the occurrence of a low energy NCol state for medium-size clusters, which depends on the specific arrangement of Cr atoms. Within the range of cluster sizes considered here, we note from Fig. 4 that all the clusters characterized by a dominant fraction of atoms with either 4 or 6 Cr nn exhibit metastable NCol configurations (N_{Cr} = 15, 24, 22, 41 and 70). In these configurations, the local moments of Cr atoms in the smaller clusters (N_{Cr} = 15, 22) all show rather small deviations from collinearity with respect to the moments of Fe atoms. In the larger clusters with a

non-negligible fraction of bulk-like Cr atoms, the local moments on the outer Cr atoms (with 4 Cr *nn*) show relatively small deviation from collinearity, whereas the moments of the inner Cr atoms have orientations almost perpendicular to the Fe moments (Fig. 5).

It is also worth mentioning that Fe local moments remain practically unchanged, and remain ferromagnetically ordered, for all the Col and NCol Cr cluster configurations explored in this study. The variation of magnetic properties of Cr clusters as a function of cluster size can therefore be primarily correlated with the magnitude and orientation of Cr magnetic moments. For instance, the magnitudes of moments averaged over all the Cr atoms for all the clusters are shown in Table II. All the clusters, including those exhibiting a NCol local minimum in addition to the Col configuration, show particularly low average magnitudes of moments in the Col state, which is a signature of magnetic frustration. There are two ways for the clusters to partially release the frustrations, either by developing NCol magnetic states or by reducing the magnitude of moments on the most frustrated Cr atoms while keeping all the Cr moments collinear with the Fe moments (Fig. 6). It appears that in the case of Cr clusters it is the second alternative that gives rise to lower-energy states for all the clusters considered here.

B. Fe clusters in AF bcc Cr

Similarly to the case of Cr clusters in Fe, we now investigate the ground state magnetic configurations of Fe clusters in AF bcc Cr. We consider small Fe clusters with N_{Fe} = 2 to 5 (Fig.7), octahedral clusters with N_{Fe} = 6, 15, 19 and 24 (Figs. 8 and 10) with the same atomic structure as Cr clusters described in Sec. III A, and a cubic cluster containing 9 Fe atoms.

Before discussing Fe clusters, we note that magnetic frustrations is already visible for an isolated Fe atom in AF bcc Cr. A substitutional Fe atom in AF bcc Cr is magnetically frustrated, since the anti-parallel-coupling preference for both the *nn* and *nnn* Fe-Cr pairs cannot be satisfied simultaneously. Again, there are two alternative ways to partially release magnetic frustration, that is, the Fe moment remains anti-parallel to the moment of the *nn* Cr atoms and its magnitude decreases significantly, or it changes orientation and becomes non-collinear with respect to the Cr moments. The lowest-energy solution predicted by DFT is the former one, with a very small Fe moment of 0.21 μ_B (Fig. 9). There is a metastable NCol magnetic state with a slightly increased local moment, which is only 0.04 eV higher in energy, where the angles between the Fe moment and *nn* and *nnn* Cr moments are 114° and 66° respectively (Table III). Based on theoretical predictions ([20,36]), we know that it is always energetically more favourable for Fe atoms to form clusters than to stay isolated in the Cr lattice. It is expected that the very strong magnetic frustration of single Fe atoms, reflected by their much smaller local moment compared with the Fe moments in clusters (Fig. 9), contribute to the clustering preference.

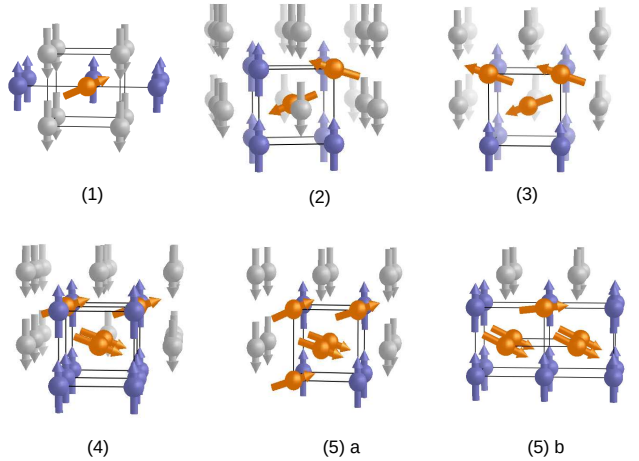

FIG. 7: Schematic representations of atomic positions and magnetic moments (arrows) for the lowest-energy NCol state of a single Fe atom and small Fe clusters in AF bcc Cr. Yellow and grey spheres denote Fe and Cr atoms, respectively. Fe cluster sizes, N_{Fe}, are given in parentheses.

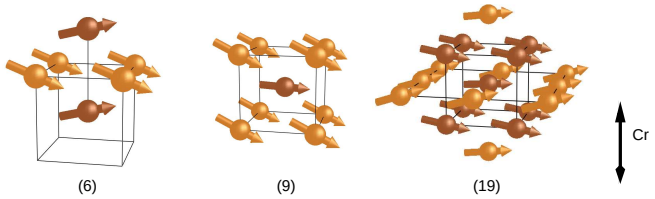

FIG. 8: Schematic representations of atomic positions and magnetic moments (arrows) for the lowest-energy NCol state of Fe clusters with N_{Fe} = 6, 9, and 19, in AF bcc Cr. Fe cluster sizes (N_{Fe}) are given in parentheses. Orientations of AF-ordered moments of Cr atoms are shown by the up-down arrow.

In comparison with Cr clusters, more energy minima corresponding to distinct magnetic states are found for Fe clusters in AF Cr. This may be rationalized by the fact that magnetism of Cr atoms is very sensitive to neighboring Fe atoms, in other words, it is largely determined by the local chemical environment. On the other hand, magnetism of Fe clusters is mainly determined by strong Fe-Fe FM coupling, and it is less sensitive to interaction with Cr atoms. Moreover, in bcc lattice, Fe shows stronger tendency to becoming magnetic than Cr, attested by a larger energy difference between FM and NM (non-magnetic) states of Fe (0.54 eV/atom) compared to a much small difference between AF and NM states of Cr (0.03 eV/atom)[33]. Such differences are directly reflected in the magnitudes of local moments on Cr and Fe atoms in the respective clusters. In Cr clusters, the

N_{Fe}	Angle (°)
1	114
2	107, 112
3	109(x2), 110
4	109(x2), 110(x2)
5a	108(x4), 113
5b	96, 116(x4)
6	103(x2), 112(x4)
9	116(x8), 93(central)
19	107(x8), 97(x2), 101(x8), 87(central)

TABLE III: Angles between Fe atomic moments in the clusters and Cr *nn* moments for various cluster sizes (N_{Fe}). Cluster configurations are shown in Figs 7 and 8. The number of Fe atoms with the same orientation of moments is shown in parentheses. The angle for the central atom in the 9- and 19-atom clusters is defined in the same coordinate system as for its 8 Fe *nn* neighbour atoms.

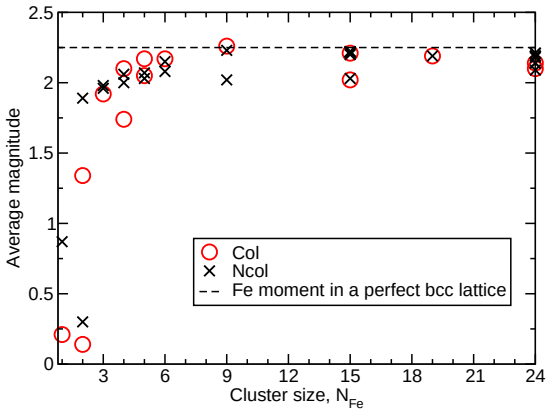

FIG. 9: Average magnitude of local magnetic moments (in μ_B units), computed for various Col and NCol configurations, shown for all the Fe clusters included in this study. Magnitude of a Fe atom moment in bcc FM lattice is shown for comparison.

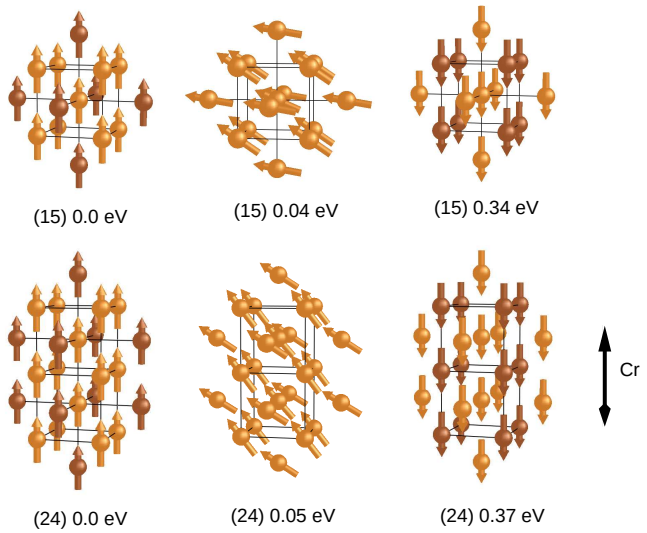

FIG. 10: Schematic representation of atomic positions and local magnetic moments (arrows) of Fe clusters of 15 and 24 atoms in AF bcc Cr. Two Col (left and right) and an intermediate-energy NCol (middle) configurations are shown together the difference between their energy and that of the ground state. In the Col states, the light yellow atoms have local moments anti-parallel to their *nn* Cr atoms. The Fe cluster size is given in parentheses. Orientation of the lattice Cr atoms is also shown.

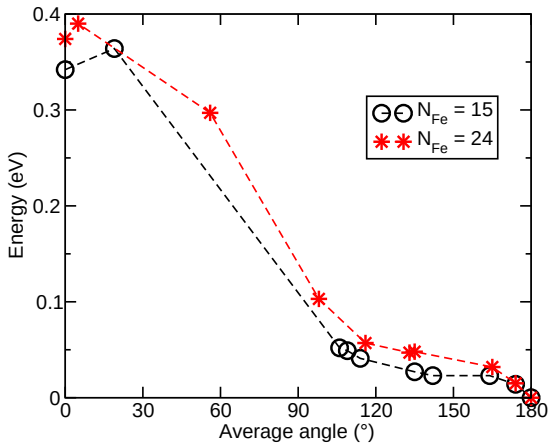

FIG. 11: 15- and 24-Fe clusters in AF bcc Cr: energy of a magnetic configuration with respect to the magnetic ground state, computed for various Col and NCol states versus the average angle of Fe local magnetic moments. States with angle = 180° and 0° correspond to Col states (shown on the left and right panels of Fig. 10).

magnitudes of local moments often differ significantly between atoms in a cluster and between different clusters (see Table II and Fig. 6). On the other hand, for Fe clusters, we note that the magnitudes of atomic moments on all the Fe atoms in a cluster are fairly similar, and the average magnitude of atomic moment in a cluster converges already to the magnitude of bcc bulk Fe moment (2.25 μ_B), even for relatively small cluster sizes (Fig. 9). Such differences between Fe and Cr are expected to result in dissimilar behaviour of Fe and Cr clusters, especially if some of the atoms are magnetically frustrated. In general, Fe atoms develop NCol configurations much more readily, as shown below, whereas Cr atoms tend to adopt collinear configurations characterized by fairly small atomic moments.

We consider three possible magnetic configurations of a Fe dimer ($N_{Fe} = 2$): (i) the two Fe moments are parallel to each other and collinear to the Cr moments, (ii) moments of the two Fe atoms are anti-parallel to each other, and both are anti-parallel to the moments of their respective *nn* Cr atoms, and (iii) the two Fe atoms are non-collinear with respect to each other and the Cr lattice. The latter configuration is in fact the lowest-energy state, exhibiting the largest atomic moments. The first

and second configurations are, respectively, 0.04 eV and 0.07 eV above the ground state. The average magnitudes of Fe moments for the three cases are, respectively, 1.34 μ_B, 0.30 μ_B and 1.89 μ_B. Note that states (i) and (ii) favor FM coupling between the two Fe atoms and AF coupling between the *nn* Fe-Cr pairs. The NCol configuration (state (iii)) gives the best compromise between all the FM Fe-Fe, and *nn* and *nnn* AF Fe-Cr magnetic interactions. In this NCol state, the angle between the two Fe local moments is 39°, whereas the angles between the Fe moment and the moments of their respective Cr *nn* are 107° and 112° (Table III).

In comparison with Cr clusters in Fe, all the small Fe clusters in Cr studied here, with N_{Fe} = 2 to 5, exhibit non-collinear magnetic configurations as the lowest-energy states. Energy difference between the lowest-energy collinear and non-collinear states are 0.06 eV, 0.09 eV, 0.07 eV and 0.05 eV, respectively, for the 3-, 4-, 5a- and 5b-clusters shown in Fig. 7. In these clusters, all the Fe atoms have at least four Cr *nn*. As was noted in relation to a Fe dimer, non-collinear arrangements allow to reconcile, as much as possible, the competing magnetic coupling tendencies between the neighboring Fe-Fe and Fe-Cr pairs. The resulting atomic moment orientations are also similar to the Fe dimer case, that is, local moments on the Fe atoms are at angles of up to 39° with respect to each other, and at angles varying from 108° to 116° with respect to the *nn* Cr moments (Table III). The central atom of a 5-Fe cluster in (b) configuration (Fig.7) presents a special case. The moment of this, very frustrated, Fe atom is nearly perpendicular (the angle is 96°) to the moment of its four Fe *nn* and of its four Cr *nn*.

Non-collinear magnetic ground states gradually vanish in the limit of large Fe clusters. In terms of competition between the Fe-Fe FM coupling and Fe-Cr AF coupling tendencies, the former becomes dominant with increasing cluster size. Consistently, we find that collinear states are either very close or lower in energy than the non-collinear states. For instance, for the cubic cluster with N_{Fe} = 9, and for the octahedral clusters with N_{Fe} = 6 and 19, the energetically most favourable non-collinear states (Fig. 8) are only 0.03 eV, 0.01 eV and 0.02 eV lower in energy than the corresponding collinear states. These energy differences are within the uncertainty margin of DFT predictions. Therefore, in practice the Col and NCol states can be treated as degenerate. In the NCol states, the maximum angles between Fe moments are 35°, 23°, and 18°, respectively, for the 6-, 9- and 19-Fe clusters. The angles between Fe and *nn* Cr moments are given in Table III, varying from 97° to 116°, similar to the smaller cluster cases.

For other medium-size but more compact clusters (N_{Fe} = 15 and 24), where all the Fe atoms have at least and mainly four Cr *nn*, the FM tendency between Fe atoms dominates. Consequently, the lowest-energy state is a collinear configuration, where most of the Fe atoms (9 over 15 and 14 over 24) are not magnetically frustrated with respect to their *nn* Cr atoms, as shown in the left plots of Fig. 10. Many non-collinear states exist as local energy minima. Relative energies of such states are shown in Fig. 11. Note that many of the NCol states are less than 0.05 eV above the Col ground state. Therefore there is high probability of such non-collinear states being occupied even at relatively low temperatures.

IV. MCE RESULTS AND DISCUSSION

A. Cr clusters in Fe

Equilibrium magnetic structures of Cr clusters in Fe matrix were explored using Magnetic Cluster Expansion simulations[24,25,29]. All the clusters studied by DFT calculations were also investigated by MCE. Also, we studied larger clusters that cannot be treated using the relatively small DFT supercells. The two types of larger clusters are the cubic clusters with six (100) interfaces and octahedral clusters with eight (110) interfaces. Following the notations used in Table I, a cubic cluster can be represented as $2n-1$ layers with a general formula n^2-$(n-1)^2$-n^2-...-$(n-1)^2$-n^2, where the total number of atoms is $n^3+(n-1)^3$. For the octahedral clusters with (110) interfaces, the general formula is 1^2-2^2-...-n^2-$(n-1)^2$-...-1^2, with the total number of atoms in the cluster being $(2n^3+n)/3$. For the cubic clusters, the following sizes were included: 9, 35, 91, 189, 341, 559, 855, and 1241 Cr atoms in Fe matrix. Octahedral clusters of size 6, 19, 44, 85, 146, 231, 344, 489, 670, 891, 1156, and 1469 Cr atoms in Fe matrix were also investigated. Simulations were performed using a supercell containing 16000 atoms (20x20x20 bcc unit cells) for both types of clusters.

First, in order to compare our simulations with DFT calculations, an extensive search for a global minimum as well as for possible metastable magnetic configurations was conducted. Simulations were performed assuming that moments change their directions, and also with moments constrained to collinearity. Since the energy differences between noncollinear and collinear magnetic configurations can be very small, especially for small Cr clusters, a three-stage quenching was performed from temperature T=1000 K to T=1 K (first stage), 10^{-3} K (second stage), and 10^{-6} K (third stage).

Summarizing our results, we found that in small clusters Cr atoms retain collinearity with respect to the Fe environment. Simulations with and without the collinearity constraint converged to the same (collinear) configurations for clusters containing up to 5 atoms, as well as for 6-atomic octahedral and 9-atomic cubic cluster. All the clusters with 13 and more Cr atoms studied here have non-collinear magnetic ground states. Energy difference between the non-collinear ground state and the ground state obtained with collinearity constraint is the lowest for cubic clusters. For example, for a 35-atomic cluster, the energy of a non-collinear configuration is only

0.22 meV per Cr atom lower than that of a collinear configuration. For the octahedral and mixed clusters, the difference between energies is larger, approaching 24.5 meV per Cr atom for a 19-atom cluster (Figure 12). The emergence of magnetic non-collinearity in cubic clusters is illustrated in Figure 13, where we plot two components of magnetic moments of Cr atoms, parallel and orthogonal to bulk Fe atoms for the three smallest cubic clusters. For a 9-atom cluster, moments are completely collinear to the Fe moments.

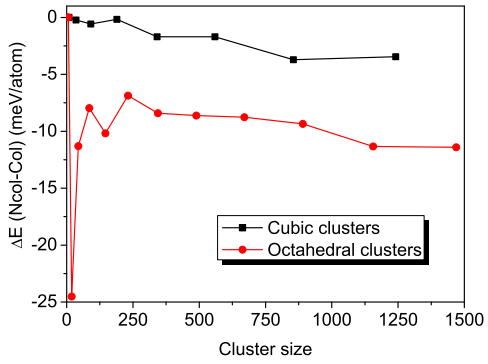

FIG. 12: Energy difference between the non-collinear ground states and ground states found under the collinearity constraint for cubic and octahedral chromium clusters, meV per Cr atom.

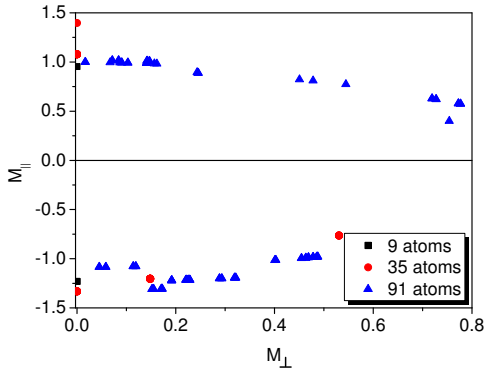

FIG. 13: Parallel and orthogonal components of Cr magnetic moments computed for the three smallest cubic clusters investigated by MCE.

The dependence of the tilt angle (with respect to the bulk Fe magnetization) and the magnitude of Cr moments on the number of their nearest Cr neighbors for small cubic and octahedral clusters (35 and 44 Cr atoms, respectively) is shown in Figure 14. According to Figure 14a, the moments of atoms with fewer than three Cr atoms in the nearest neighbor shell are almost completely collinear and anti-parallel to the moment of iron lattice. Strong deviation from collinearity is found for atoms with four nearest Cr neighbors in cubic, and with five Cr neighbors in octahedral clusters, respectively. Atoms that are inside the two clusters and have 8 Cr among their nearest neighbours are strongly influenced by the large number of collinear Cr atoms at the cluster-matrix interface and hence are close to collinearity themselves, with their moments being almost parallel to the moments of iron atoms. The magnitude of magnetic moment exhibits a minimum for atoms with four to six nearest Cr neighbors (Figure 14b). This reduction of the local moment coincides with strong tilting away from collinearity and represents another way of releasing magnetic frustration, similar to the one found in DFT studies of Fe clusters in Cr (see above, Sec. IIIB). In the bulk of Cr clusters, the magnitude of magnetic moments of Cr atoms increases.

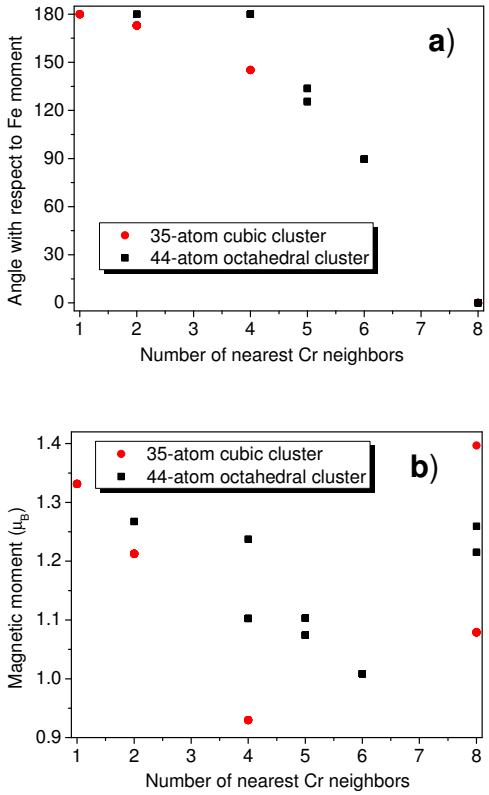

FIG. 14: Angle between Fe magnetic moment and moments of Cr atoms in small cubic and octahedral clusters plotted as a function of the number of nearest Cr neighbors (a). The magnitude of magnetic moment of Cr atoms in small cubic and octahedral clusters plotted as a function of the number of nearest Cr neighbors (b).

Magnetic moments of Cr atoms in the clusters for which non-collinear solutions were found in DFT calculations are shown in Figure 15. They all are found to be non-collinear in MCE simulations. Energy gains of non-

collinear compared to collinear magnetic configurations are 4.195, 0.408, 1.044, 5.369, and 7.191 meV per Cr atom for 15, 22, 24, 41, and 70-atomic clusters, respectively.

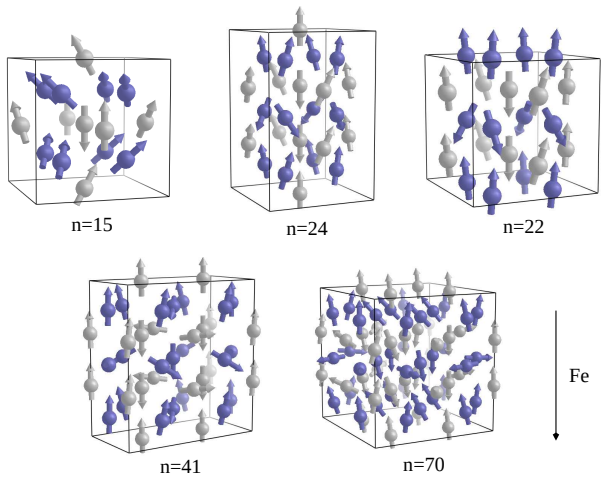

FIG. 15: Schematic representation of atomic positions and local magnetic moments (arrows) of Cr clusters containing 15, 24, 22, 41 and 70 atoms found in MCE simulations. Orientation of the FM ordered Fe moments is also shown.

Variation of magnetic moments of Fe atoms at the Cr cluster interface was also investigated. Near Cr clusters, iron moments are smaller than in the bulk, in agreement with our analysis of Fe/Cr interfaces[22] and calculations by Alvarado et al.[38]

Temperature dependence of cluster energy for large cubic and octahedral chromium clusters is shown in Figure 16. Results are normalized to a single cluster atom. We see that the energy plotted as a function of temperature shows the same features that were found for Fe-Cr interfaces, namely that it decreases at temperatures corresponding to magnetic transitions, the Neel temperature of Cr (310 K) and the Curie temperature of Fe (1043 K). Also, the relative energy of cubic and octahedral clusters follows the trend shown in Fig. 12 of Ref.[22], namely that an octahedral cluster with (110) interfaces has higher energy per Cr atom at low temperatures, but the relative stability of octahedral and cubic (with (100) interfaces) clusters changes near the Curie transition temperature.

Due to anti-ferromagnetic coupling between Fe and Cr moments at the cluster-matrix interface, the ferromagnetic iron matrix induces non-vanishing magnetization in chromium clusters. For small clusters, the average moment per Cr atom can be as high as $1\mu_B$, i.e. it approaches the absolute magnitude of Cr magnetic moment. We studied the dependence of this parameter on the cluster size as well as on temperature. The cluster size dependence of the average magnetic moment per Cr atom is similar for cubic and octahedral clusters, as seen in Figure 17. If the overall magnetization, treated as a function of cluster size N, were proportional to the fraction of Cr atoms at the cluster surface ($\sim N^{2/3}$), the

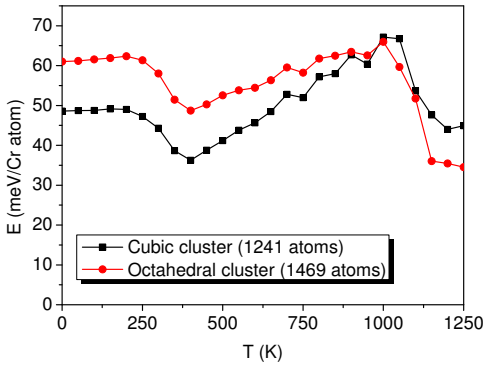

FIG. 16: Energy per Cr atom in chromium clusters (1241-atomic cubic cluster and 657-atomic octahedral cluster) as a function of temperature.

magnetization per Cr atom could be approximated as $N^{-1/3}$. Our fit gives the power law for the magnetization per atom very close to $N^{-2/5}$ (the exponents being -0.40652 for cubic and -0.42058 for octahedral clusters, respectively), showing that in fact magnetization decreases slightly faster than $N^{-1/3}$. The total induced magnetization of a cluster varies as a function of the number of atoms in the cluster as $N^{3/5}$. The overall magnetization of Cr clusters induced by the surrounding Fe atoms vanishes only at high temperature, comparable with the Curie temperature of Fe (see Figure 18).

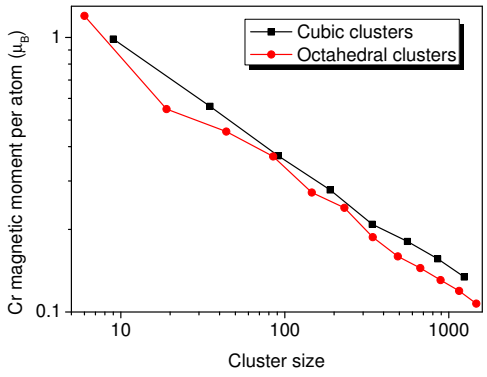

FIG. 17: Magnetization of Cr clusters, per atom, plotted vs cluster size for cubic and octahedral clusters.

To investigate temperature dependence of magnetic properties of clusters we analyzed the nearest neighbor Cr-Cr anti-ferromagnetic correlations, defined as

$$C_{nn} = \frac{1}{N_{nn}} \sum_{i,j \in nn} \frac{\mathbf{M}_i \cdot \mathbf{M}_j}{|\mathbf{M}_i||\mathbf{M}_j|}. \qquad (2)$$

For cubic clusters, correlation function C_{nn} is shown in Figure 19 together with the correlation function com-

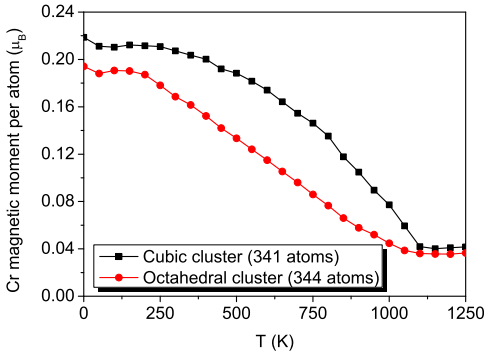

FIG. 18: Temperature dependence of magnetization of cubic (341 atoms) and octahedral (344 atoms) Cr clusters.

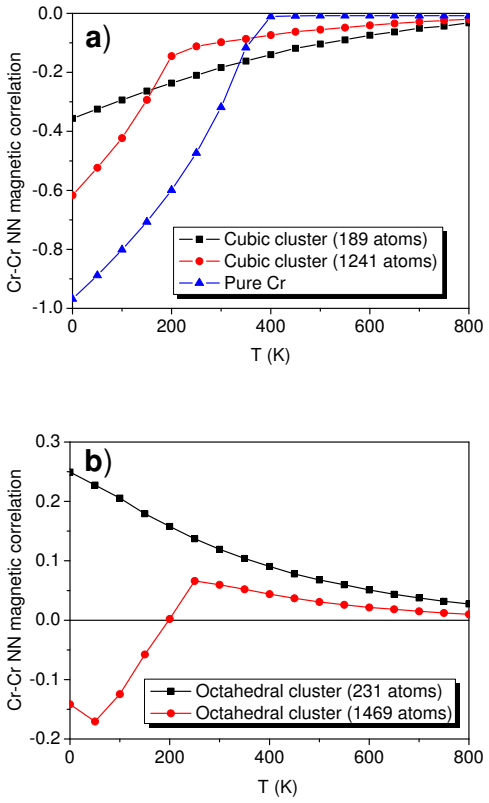

FIG. 19: Anti-ferromagnetic correlations in cubic Cr clusters (a) and octahedral Cr clusters (b).

puted for pure Cr. For the relatively small 189-atom cluster correlations are not very strong, but they persist until relatively high temperatures, higher than the Néel temperature of Cr. This is due to the anti-ferromagnetic coupling of atoms at the cluster interface with the Fe matrix, which helps to preserve magnetic order inside the cluster

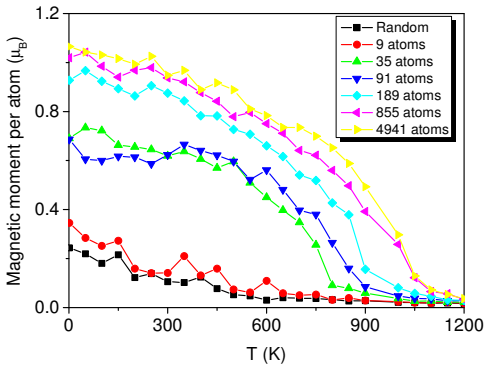

FIG. 20: Magnetic moment per atom plotted as a function of temperature for Fe-40 at.% Cr alloys. Chromium atoms are either distributed randomly in Fe matrix, or form a mixture of cubic nano-clusters of various sizes suspended in Fe-12 at.% random alloy (see text).

even at high temperatures. For the large 1241-atom cluster, correlations at low temperatures are stronger, but they decrease faster with temperature. This behavior is closer to what is found for pure chromium. Temperature dependence of correlations is more interesting in octahedral clusters (Figure 19b). For a small 231-atom cluster, correlations turn out to be positive in the entire range of temperatures. For the large 1469-atom cluster, correlations are anti-ferromagnetic at low temperatures, but they change sign at temperatures close to the Néel temperature of Cr. This unusual behavior can be explained if we note that in octahedral clusters, unlike in cubic clusters, there is a large fraction of nearest-neighbor bonds between pairs of Cr atoms situated at the interface between the cluster and the matrix (in cubic clusters, there are no such bonds). In a 231-atom octahedral cluster, 576 out of 1256 (45.9%) nearest-neighbor bonds involve interfacial atoms, whereas for the 1469-atom cluster the fraction is 2304 out of 9432 (24.4%). Interfacial Cr atoms prefer anti-parallel, with respect to the Fe matrix, orientation of magnetic moments, and as a result they are parallel to each other, despite the fact that Cr-Cr interactions are anti-ferromagnetic. This effect appears stronger in small clusters, but even in a large 1469-atom cluster, anti-parallel Fe-Cr interaction dominates over the anti-parallel Cr-Cr interaction near the Néel temperature of Cr.

In order to study how magnetization of an alloy with high Cr content depends on both temperature and solute cluster size, we performed simulations for several Fe-Cr systems, consisting of a mixture of cubic chromium clusters and random Fe-Cr alloy. The configurations were created as follows: for a given cluster size, Cr clusters were randomly distributed in the simulation box. The rest of the box contained Fe-12 at.% Cr random solution. The total amount of chromium atoms in the system was

kept at 6400, corresponding to 40 at.% Cr. Also, fully random Fe-40 at.% Cr mixture was investigated. Figure 20 shows the temperature dependence of magnetization for a random alloy and alloys with different cubic cluster sizes, starting with 566 9-atom Cr clusters and finishing with a single cluster consisting of 4941 Cr atoms. The Fe-Cr random mixture and alloy containing 9-atom clusters show almost identical temperature dependence with magnetization approaching zero at about 600K. For larger 35- and 91-atom Cr clusters, low-temperature magnetization is higher and it vanishes at higher temperatures of 800-900K. Finally, starting from 189-atomic clusters, the magnetization behaviour changes only slightly with increasing clusters size, and magnetization vanishes at temperatures which are close to the Curie temperature of pure iron (1043 K).

Results shown in Figure 20 can be discussed in relation to the experimental study by Yamamoto[9], although a direct comparison is hardly possible. Figure 3 of Ref. 9 shows variation of magnetization vs temperature for several Fe-Cr specimens quenched from 1100°C and annealed at 500°C. For specimens with more than 38 wt% Cr, the difference between magnetization curves is very prominent. The quenched specimens show a sluggish decrease of magnetization with temperature, while for the annealed specimens, a sharp drop in magnetization is observed above 550°C (820-830 K). The author of Ref. 9 attributes this sharp drop to a phase transformation in Fe-Cr, presumably a transition from clustered to a random solution phase above the miscibility gap. In our simulations, this would correspond to a sharp transition from the plots corresponding to large (189 and more Cr atoms) clusters in Figure 20 to a plot corresponding to a completely random solution, with the corresponding rapid decrease in magnetization. On the other hand, heating of a quenched system with 46.5 wt% Cr results in, according to Ref. 9, (i) the Curie transition at 380° C (close to our prediction of 600 K for a random alloy) and (ii) diffusion-related precipitation of chromium at higher temperature, ending in the complete disappearance of magnetization above 550°C, like in the case of annealed specimens. A direct comparison between experiment and simulations is not possible since in the simulations thermally activated diffusion of Cr atoms is not taken into account (Cr atoms do not change posotion in the simulation cell).

Overall, magnetic non-collinearity of Cr clusters in Fe appears to have the same origin as non-collinearity found at Fe/Cr interfaces[22], namely that it results from magnetic frustration occurring due to competition between anti-ferromagnetic *nn* and *nnn* Fe-Cr interactions and anti-ferromagnetic *nn* Cr-Cr interactions. However, in Cr clusters the picture is more complex than at interfaces, because in clusters there is preferred direction along which magnetization and other properties change (at an interface, such direction is provided by the vector normal to the interface). In a cluster, the magnetic state of each Cr atom depends on its distance from several interfaces, and a simple model developed in[22], as a criterion for magnetic non-collinearity, cannot be directly applied here.

B. Fe clusters in Cr

For a single Fe atom in Cr, Monte Carlo simulations predict the angle between Fe magnetic moment and Cr moments of about 130°. This does not agree with DFT results where collinear magnetic structure (with the angle relative to the moment of the nearest Cr atoms is 180°) with a very small Fe magnetic moment has the lowest energy. At the same time, the angle of 130° is intermediate between the collinear DFT solution and the noncollinear one, where the corresponding angle is 114°. Energy gain of non-collinear configuration relatively to the collinear one for a single Fe atom is 32 meV. The magnitude of Fe magnetic moment in both non-collinear and collinear solutions is reduced compared to bulk iron, but not as strongly as in DFT calculations: the moment of the Fe atom is 1.584 μ_B for non-collinear and 1.480 μ_B for collinear magnetic configurations.

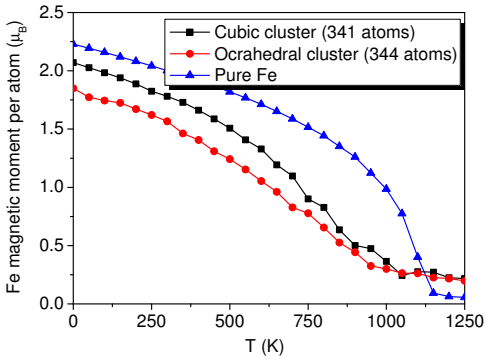

FIG. 21: Temperature dependence of the overall magnetization for cubic (341 atoms) and octahedral (344 atoms) Fe clusters, and the magnetization of pure iron.

Here, we again have the case of MCE predicting an intermediate ground state between collinear and non-collinear DFT solutions, similarly to the case of small Cr clusters in Fe. For a two-atom Fe cluster, the magnitude of moments at each Fe atom is 1.65 μ_B, i.e. it increases in comparison with a single Fe atom case. The moments of the two Fe atoms are almost parallel to each other (the angle between them is 9°). With increasing cluster size, the magnitude of magnetic moment of Fe atoms increases, but more slowly than in DFT calculations (see Figure 9). For the 5-atom cluster, the magnitude of moment on a Fe site is 1.73 μ_B. The angle between the average Fe moment in a cluster and the moment of Cr atoms in the matrix does not exhibit any systematic trend with increasing Fe cluster size, still these moments are always

close to being orthogonal to each other. Non-collinear configurations are always more stable that configurations calculated with collinear constraint, with the energy gain being the largest for a 3-atom cluster (160 meV/atom).

For a 9-atom cubic Fe cluster, the average magnitude of Fe moments at the cluster-matrix interface is 1.79 μ_B. This value increases towards the bulk value with increasing cluster size, reaching 2.13 μ_B for the largest studied 1241-atomic cubic Fe cluster. Similar behavior is observed for the octahedral iron clusters, where the average magnetic moment on Fe atoms increases from 1.76 μ_B for the 6-atom to 2.12 μ_B for the 1469-atom cluster.

To study temperature effects, we computed the total magnetization of cubic and octahedral clusters as a function of temperature, and compared results with magnetization of pure Fe (Figure 21). For low temperatures, non-collinearity results in decreasing magnetization, which is more pronounced for the octahedral clusters. At higher temperatures, the magnetization of clusters decreases somewhat more rapidly than that of the pure Fe, which can be explained by disordering of Cr moments above the Néel temperature. Overall, we find weaker temperature variation of magnetization of Fe clusters compared to that of Cr clusters in iron. This can be explained by strong Fe-Fe magnetic interaction and relatively weak influence of Cr surrounding.

V. CONCLUSIONS

First principles and MCE Monte Carlo studies were performed to investigate the lowest-energy magnetic configurations and finite temperature magnetic properties of Cr clusters in FM bcc-iron and Fe clusters in AF bcc-Cr. In particular, we studied very small clusters, and those with (100) and/or (110) interfaces.

We showed, by means of non-collinear DFT calculations, that magnetic frustration caused by competing Fe-Fe, Fe-Cr and Cr-Cr magnetic-coupling tendencies determines the low-energy magnetic configurations of the clusters, inducing the appearance of either small local magnetic moments or non-collinear structures, which partially release magnetic frustration. Small local atomic moments are often found in collinear ground states of Cr clusters in Fe. Non-collinear configurations are unstable for most of the studied Cr clusters, except for the clusters where interfacial Cr atoms dominate the structure, with either four or six Cr nearest neighbors, in which case non-collinear states exist as metastable local minima. A particularly interesting feature concerns the non-zero cluster magnetization caused by the dominance of Fe-Cr over Cr-Cr AF coupling in small and medium-size Cr clusters.

As opposed to the case of Cr clusters in Fe, non-collinear configurations commonly occur in Fe clusters, where they form as a way of alleviating magnetic frustration. In particular, non-collinear ground states are observed if the cluster size is sufficiently small ($N_{Fe} \leq 5$) so that Fe-Cr AF coupling competes with or even dominates over Fe-Fe FM interactions. For larger clusters, all the Fe local moments remain parallel to each other. The energies of various collinear and non-collinear are generally not very dissimilar.

MCE simulations broadly agree with DFT analysis, especially for the low-energy magnetic structures, and enable extending DFT results to much larger clusters and finite temperature effects.

We found that the smallest Cr clusters in Fe matrix have collinear magnetic structure. Non-collinearity begins to appear at cluster sizes of at least 13 Cr atoms, and for smaller clusters deviations from collinearity are smaller than for larger ones. Energy gain from adopting a non-collinear ground state compared to the collinear state is smaller for cubic clusters than for octahedral clusters. The strongest deviation from collinearity is observed for the interfacial atoms with four or five nearest Cr neighbors, with atoms having fewer nearest Cr neighbors being almost collinear to the iron matrix. The ferromagnetically ordered Fe matrix induces nonzero total magnetic moment on the chromium clusters, which can be as high as $1\mu_B$ per atom in the limit of small cluster size.

The temperature dependence of magnetic properties of Cr clusters is strongly influenced by the Fe matrix. Strong Fe-Cr interaction results in the total magnetization of clusters remaining nonzero until high temperatures, close to the Curie temperature of pure Fe for larger clusters. Cr-Cr correlations also persist until higher temperatures due to the coupling of interfacial Cr atoms with the Fe matrix. Interesting behavior of correlations is observed for octahedral clusters, where they change sign from anti-ferromagnetic to ferromagnetic with increasing temperature. The reason for such change is a relatively large number of the nearest-neighbor bonds between interfacial Cr atoms with moments anti-parallel to Fe matrix and thus parallel to each other, especially at elevated temperatures. Temperature dependence of magnetization was also simulated for various cluster sizes and assessed against the available experimental data[9].

For small Fe clusters in Cr matrix, MCE results show that non-collinearity is the most efficient way of alleviating magnetic frustration, in agreement with DFT findings. Temperature dependence of the total cluster magnetization is not as strong, compared with the case of Cr clusters in iron.

Finally, this study shows the significance of performing magnetic calculations in the non-collinear approximation, since non-collinear configurations of Fe and Cr clusters have energies lower than, or close to, the energies of collinear states, and thus likely occur even at relatively low temperatures. This is also to be expected in any alloys composed of elements exhibiting tendencies towards FM and AF magnetic ordering.

Acknowledgments

This work was part-funded by the RCUK Energy Programme (Grant Number EP/I501045) and by the European Unions Horizon 2020 research and innovation programme under grant agreement number 633053. All the DFT calculations were performed using resources of IFERC-CSC Helios supercomputer (Japan) and GENCI project (Grant x2014096020). To obtain further information on the data and models underlying this paper please contact PublicationsManager@ccfe.ac.uk. The views and opinions expressed herein do not necessarily reflect those of the European Commission. This work was also part-funded by the United Kingdom Engineering and Physical Sciences Research Council via a programme grant EP/G050031.

[1] R. Klueh and A. Nelson, J. Nucl. Mater. **371**, 37 (2007).
[2] S. J. Zinkle and J. T. Busby, Materials Today **12**, 12 (2009).
[3] S. L. Dudarev, J. L. Boutard, R. Lässer, M. J. Caturla, P. M. Derlet, M. Fivel, C.-C. Fu, M. Y. Lavrentiev, L. Malerba, M. Mrovec, et al., J. Nucl. Mater. **386-388**, 1 (2009).
[4] M. Bachhav, G. Odette, and E. Marquis, Scr. Mater. **74**, 48 (2014).
[5] P. Olsson, C. Domain, and J. Wallenius, Phys. Rev. B **75**, 014110 (2007).
[6] E. Martinez, O. Senninger, C. Fu, and F. Soisson, Phys. Rev. B **86**, 224109 (2012).
[7] R. Soulairol, C.-C. Fu, and C. Barreteau, Phys. Rev. B **83**, 214103 (2011).
[8] H. Wen, P.-W. Ma, and C. H. Woo, J. Nucl. Mater. **440**, 428 (2013).
[9] H. Yamamoto, Japan. J. Appl. Phys. **3**, 745 (1964).
[10] A. Bergman, L. Nordstrom, A. Klautau, S. Frota-Pessa, and O. Eriksson, Phys. Rev. B **75**, 224425 (2007).
[11] V. Stepanyuk, W. Hergert, P. Rennert, K. Kokko, A. Tatarchenko, and K. Wildberger, Phys. Rev. B **57**, 15585 (1998).
[12] R. Igarashi, A. Klautau, R. Muniz, B. Sanyal, and H. Petrilli, Phys. Rev. B **85**, 014436 (2012).
[13] R. Robles and L. Nordstrom, Phys. Rev. B **74**, 094403 (2006).
[14] D. Nguyen-Manh and S. L. Dudarev, Phys. Rev. B **80**, 104440 (2009).
[15] R. Longo, A. Vega, S. Bouarab, M. Ferrer, J. Alemany, and L. Gallego, Phys. Rev. B **77**, 212406 (2008).
[16] D. Nguyen-Manh, M. Y. Lavrentiev, and S. L. Dudarev, J. Computer-Aided Mater. Des. **14**, 159 (2007).
[17] D. Nguyen-Manh, M. Y. Lavrentiev, and S. L. Dudarev, C. R. Acad. Sci. Paris **9**, 379 (2008).
[18] O. Senninger, E. Martinez, F. Soisson, M. Nastar, and Y. Brechet, Acta Mater. **73**, 9 (2014).
[19] T. P. C. Klaver, R. Drautz, and M. W. Finnis, Phys. Rev. B **74**, 094435 (2006).
[20] M. Levesque, E. Martinez, C. Fu, M. Nastar, and F. Soisson, Phys. Rev. B **84**, 184205 (2011).
[21] A. Kiejna and E. Wachowicz, Phys. Rev. B **78**, 113403 (2008).
[22] M. Y. Lavrentiev, R. Soulairol, C.-C. Fu, D. Nguyen-Manh, and S. Dudarev, Phys. Rev. B **84**, 144203 (2011).
[23] H. Fritzsche, S. Bonn, J. Hauschild, J. Klenke, K. Prokes, and G. McIntyre, Phys. Rev. B **65**, 144408 (2002).
[24] M. Y. Lavrentiev, S. Dudarev, and D. Nguyen-Manh, J. Nucl. Mater. **386-388**, 22 (2009).
[25] M. Y. Lavrentiev, D. Nguyen-Manh, and S. L. Dudarev, Phys. Rev. B **81**, 184202 (2010).
[26] M. Y. Lavrentiev, S. Dudarev, and D. Nguyen-Manh, J. Appl. Phys. **109**, 07E123 (2011).
[27] M. Y. Lavrentiev, K. Mergia, M. Gjoka, D. Nguyen-Manh, G. Apostolopoulos, and S. L. Dudarev, J. Phys. Condens. Matter **24**, 326001 (2012).
[28] M. Y. Lavrentiev, J. S. Wróbel, D. Nguyen-Manh, and S. Dudarev, Physical Chemistry Chemical Physics **16**, 16049 (2014).
[29] M. Y. Lavrentiev, D. Nguyen-Manh, and S. Dudarev, Solid State Phenom. **172-174**, 1002 (2011).
[30] J. Soler, E. Artacho, J. Gale, A. Garcia, J. Junquera, P. Ordejón, and D. Sanchez-Portal, J. Phys. Condens. Matter **14**, 2745 (2002).
[31] V. García-Suárez, C. Newman, C. Lambert, J. Pruneda, and J. Ferrer, J. Phys. Condens. Matter **16**, 5453 (2004).
[32] J. Perdew, K. Burke, and M. Ernzerhof, Phys. Rev. Lett. **77**, 3865 (1996).
[33] R. Soulairol, C.-C. Fu, and C. Barreteau, J. Phys. Condens. Matter **22**, 295502 (2010).
[34] R. Soulairol, C.-C. Fu, and C. Barreteau, Phys. Rev. B **84**, 155402 (2011).
[35] J. Sanchez, F. Ducastelle, and D. Gratias, J. Nucl. Mater. **128**, 334 (1984).
[36] M. Y. Lavrentiev, R. Drautz, D. Nguyen-Manh, T. P. C. Klaver, and S. L. Dudarev, Phys. Rev. B **75**, 014208 (2007).
[37] M. Y. Lavrentiev, D. Nguyen-Manh, and S. Dudarev, Comp. Mater. Sci. **49**, S199 (2010).
[38] P. Alvarado, J. Dorantes-Davila, and G. Pastor, Phys. Rev. B **58**, 12216 (1998).